A nonequilibrium binary elements-based kinetic model for benzodiazepine regulation of $GABA_A$ receptors

Marcel P. Goldschen-Ohm,[1] Alexander Haroldson,[1] Mathew V. Jones,[1] and Robert A. Pearce[2]

[1]Department of Neuroscience and [2]Department of Anesthesiology, University of Wisconsin, Madison, WI 53706

Ion channels, like many other proteins, are composed of multiple structural domains. A stimulus that impinges on one domain, such as binding of a ligand to its recognition site, can influence the activity of another domain, such as a transmembrane channel gate, through interdomain interactions. Kinetic schemes that describe the function of interacting domains typically incorporate a minimal number of states and transitions, and do not explicitly model interactions between domains. Here, we develop a kinetic model of the $GABA_A$ receptor, a ligand-gated ion channel modulated by numerous compounds including benzodiazepines, a class of drugs used clinically as sedatives and anxiolytics. Our model explicitly treats both the kinetics of distinct functional domains within the receptor and the interactions between these domains. The model describes not only how benzodiazepines that potentiate $GABA_A$ receptor activity, such as diazepam, affect peak current dose–response relationships in the presence of desensitization, but also their effect on the detailed kinetics of current activation, desensitization, and deactivation in response to various stimulation protocols. Finally, our model explains positive modulation by benzodiazepines of receptor currents elicited by either full or partial agonists, and can resolve conflicting observations arguing for benzodiazepine modulation of agonist binding versus channel gating.

The Journal of General Physiology

INTRODUCTION

Ion channels are specialized proteins composed of multiple structural domains that regulate the passage of ions across cell membranes. To accomplish this task, they undergo structural rearrangements between conducting and nonconducting states that are initiated or influenced by external signals such as transmembrane voltage or ligand binding. In many cases these signals are known to impinge on structural domains separate from those comprising the channel gate, where they influence channel gating via interactions between domains. Of particular clinical interest is the ability of ion channels, as well as enzymes and many other proteins, to bind ligands that allosterically modulate their activity. This characteristic has made them important drug targets for human disease therapies (Kaczorowski et al., 2008).

Kinetic models have become important tools in the effort to understand how proteins transduce external signals into changes in activity. The standard approach is to posit a limited set of distinct functional states and specific transitions between them (e.g., Goldschen-Ohm et al., 2011). Although the rate constants in any given model encompass the interactions present in the system, without an explicit separation of interactions from the kinetics of distinct functional domains, it can be difficult to interpret whether changes in rate constants reflect changes in interactions between domains or changes in the behavior within a domain. For example, accounting for a localized modulatory stimulus such as drug binding (or any other local perturbation, such as a mutation) with widespread effects on channel function necessitates changing numerous transition rates throughout the model. In contrast, for models where interactions are distinct parameters, one could simply associate the modulator with a local perturbation in a single domain, and then let the interdomain interactions in the system dictate the resulting functional changes in every domain. Furthermore, recent work by several groups has shown that stimulus–response relationships can be used to evaluate the equilibrium energetics of a stimulus pathway (Chowdhury and Chanda, 2012, 2013; Sigg, 2013), observations for which should provide important experimental constraints on model interaction energies.

Numerous clinically important drugs, including barbiturates, benzodiazepines (BZDs), neurosteroids, and general anesthetics, modulate GABAergic inhibition in the brain (Franks and Lieb, 1994). At fast inhibitory synapses these drugs typically lead to a prolongation of inhibitory postsynaptic currents (IPSCs), an effect that has been attributed to drug modulation of postsynaptic $GABA_A$ receptor kinetics because similar changes are observed in excised

Correspondence to Marcel P. Goldschen-Ohm: marcel.goldschen@gmail.com

A. Haroldson's present address is Dart Neuroscience LLC, San Diego, CA 92131.

Abbreviation used in this paper: BZD, benzodiazepine.

The Rockefeller University Press $30.00
J. Gen. Physiol. Vol. 144 No. 1 27–39
www.jgp.org/cgi/doi/10.1085/jgp.201411183

patches exposed to brief, high-concentration pulses of GABA. The mechanisms by which these effects occur are of considerable interest, and have been investigated using both microscopic single channel and macroscopic ensemble measurements. Different drugs are reported to influence a variety of microscopic kinetic steps, including binding, pore opening, and desensitization (Twyman et al., 1989; Bai et al., 1999). This variety of effects is consistent with the presence of several different drug binding sites inferred through mutational analysis, photolabeling, and molecular modeling.

However, even for a single class of drugs, conclusions from the different approaches have sometimes been contradictory. For example, based upon the observations that the inhaled anesthetics halothane and isoflurane slowed deactivation without altering macroscopic desensitization, we concluded that these drugs slow the microscopic agonist unbinding rate (Li and Pearce, 2000; Benkwitz et al., 2004). However, other general anesthetics, including etomidate and propofol, which bind at the same or nearby transmembrane sites, increase partial agonist efficacy (O'Shea et al., 2000; Topf et al., 2003; Rüsch et al., 2004) and can directly activate receptors, particularly for receptors carrying mutations in the gating apparatus that shift the open/closed equilibrium. These latter observations implicate changes in channel gating. Similar seemingly contradictory observations have been reported for BZDs, which potentiate responses to subsaturating, but not saturating, GABA, and do not affect single channel open dwell times or brief shut times, which is consistent with altered agonist binding (Rogers et al., 1994; Lavoie and Twyman, 1996; Perrais and Ropert, 1999; Goldschen-Ohm et al., 2010). However, BZDs also increase partial agonist efficacy and gate spontaneously open mutants as expected for modulation of channel gating (Downing et al., 2005; Rüsch and Forman, 2005; Campo-Soria et al., 2006; Gielen et al., 2012; Li et al., 2013).

Here, we develop a kinetic model of the $GABA_A$ receptor, a ligand-gated ion channel that is subject to modulation by many different drugs that in clinical practice are often used in combination. Our model explicitly treats the effects of interactions not only on the system's equilibrium constants, but also on the microscopic transition rates to simulate both equilibrium and nonequilibrium behavior. Such an approach can be crucial for differentiating between possible models based on experimental observations of biologically relevant behavior that for systems such as ion channels often occur far from equilibrium. The model includes two agonist-binding sites that interact directly with two transduction elements, which in turn interact with three gates: one underlying channel activation and two producing desensitization. A BZD-binding site also interacts with one of the transduction elements, but with weaker energetics than the agonist-binding sites.

The model proposed here not only explains the detailed kinetics of activation, desensitization, and deactivation of receptor currents elicited by a variety of stimulus protocols, but also the effect of BZD-positive modulators on all of these kinetic parameters. Furthermore, the model can account for BZD modulation of the affinity and efficacy of peak current dose–response relationships for both full and partial agonists. Thus, this model can explain previous conflicting reports suggesting that BZDs modulate either GABA binding or channel gating, and may represent a more general model of drug modulation at $GABA_A$ receptors.

MATERIALS AND METHODS

Cell culture and transfection

Human embryonic kidney (HEK) 293 cells were cultured in minimum essential medium with Earle's salts (Corning) containing 10% bovine calf serum (Sigma-Aldrich) in a 37°C incubator under a 5% CO_2 atmosphere. Cells were transfected using Lipofectamine 2000 (Invitrogen) using the prescribed protocol, with 1–4 µg total of human $\alpha_1\beta_2\gamma_2$ (1:1:1 ratio) $GABA_A$ receptor subunit cDNAs in vector pcDNA3.1 (Invitrogen). Recordings were performed 24–80 h after transfection.

Patch clamp electrophysiology

Recordings from outside-out patches excised from HEK 293 cells were made at room temperature using borosilicate glass pipettes filled with (in mM): 140 KCl, 10 EGTA, 2 MgATP, 20 phosphocreatine, and 10 HEPES, pH 7.3, with KOH; osmolarity was 315 mosM, adjusted with sucrose. Patches were voltage clamped at −60 mV and placed in the stream of a multibarreled flowpipe array (Vitrodynamics) mounted on a piezoelectric bimorph (Morgan Electro Ceramics). GABA and diazepam were dissolved in the perfusion solution, which contained (in mM): 145 NaCl, 2.5 KCl, 2 $CaCl_2$, 1 $MgCl_2$, 10 HEPES, and 10 dextrose, pH 7.3, with NaOH; osmolarity was 320 mosM, adjusted with sucrose. All reagents were from Sigma-Aldrich. A computer-controlled constant current source (WPI) drove the bimorph to move solution interfaces over the patch with 10–90% exchange times of <200 µs, as measured by the liquid junction current at the open pipette tip after each experiment. Junction currents were generated by altering the ionic strength with an additional 5 mM NaCl or 1% H_2O in solutions containing GABA or diazepam, respectively.

For a given stimulus protocol, current recordings in the presence and absence of diazepam were interleaved for the same patch to allow a direct comparison of current kinetics. The same approach was used for recordings at 30 µM and 10 mM GABA to estimate the channel's concentration–response relationship. Currents were low-pass-filtered at 5 kHz with a four-pole Bessel filter and acquired at 20 kHz using an amplifier (Axopatch 200B) and digitizer (Digidata 1320A; both from Molecular Devices), controlled by AxoGraph software (Axograph Scientific) running on a Macintosh G4 (Apple Inc.).

Binary elements kinetic models

Binary elements. A system is modeled as a collection of individual elements, each of which represents a physical or functional feature. For example, in a system describing an ion channel, one element might represent an agonist binding site, another a gate, another a voltage sensor, etc. Each element can exist in either of two metastable configurations, hence their designation as "binary elements." The configuration of an element

denotes its physical or functional status, such as an agonist- or drug-binding site that is unoccupied or occupied, a gate that is closed or open, or a voltage-sensing element that sits in one position or another. For a system of N elements, there will be 2^N states representing all of the possible unique combinations of element configurations.

In the absence of any interactions, each element can flip between its configurations according to intrinsic rate constants γ and δ, which are defined by the height of a single transition state energy barrier between configurations (Fig. 1 A), according to Eyring's transition rate theory (Eyring, 1935), as

$$\gamma = \kappa\left(\frac{k_B T}{h}\right) e^{-\left(G_\ddagger - G_0\right)/k_B T} \tag{1}$$

$$\delta = \kappa\left(\frac{k_B T}{h}\right) e^{-\left(G_\ddagger - G_1\right)/k_B T}, \tag{2}$$

where G_0 and G_1 are the free energies of the element in configuration 0 or 1, respectively; $G_\ddagger$ is the free energy of the element's transition state between configurations; k_B is Boltzmann's constant; T is temperature; h is Planck's constant; and κ is a proportionality constant.

Binary elements as described above are analogous to subunits in Koshland, Nemethy, and Filmer's (KNF) description (Koshland et al., 1966) of interacting subunits. Furthermore, each ligand binding step in Monod, Wyman, and Changeux's (MWC) description (Monod et al., 1965) of cooperative ligand binding can be thought of as an additional binding site element, all of which are coupled to a single element that can exist in either a relaxed or tense configuration.

State-dependent interactions between elements. Interactions between binary elements are state dependent. That is, a particular interaction will only occur when both interacting elements adopt the appropriate configuration. Thus, for each pair of elements there are four possible interactions, one for each unique pair of configurations. Each interaction is associated with an energetic perturbation of not only those metastable states where the interaction is occurring, but also of each of the two interacting element's transition state intermediates. For example, given an interaction between element i in configuration 1 and element j in configuration 0, we define $\Delta G_{i_1 j_0}$ as the energetic perturbation caused by the interaction of those states where elements i and j adopt configurations 1 and 0, respectively. Furthermore, we define $\Delta G^{\ddagger}_{ij_0}$ as the change in free energy of element i's transition state intermediate due to its interaction with configuration 0 of element j, and $\Delta G^{\ddagger}_{ji_1}$ as the analogous change in element j's transition state when element i adopts configuration 1 (Fig. 1 B). In the absence of a change in configuration of element j, the effect of its interaction with element i's transition state is independent of whether or not element i is transitioning from configuration 0 to 1, or 1 to 0 (i.e., interactions with an element's transition state depend only on the nature of the transition state itself, not on how it got there). Thus, for example, $\Delta G^{\ddagger}_{ij_0}$ will be the same for interactions in both the i_0j_0 and i_1j_0 states (Fig. 1 B). Finally, interactions are assumed to be independent of each other, such that the energies of multiple simultaneous interactions are additive.

For any pair of binary elements i and j, there are four possible states (i_0j_0, i_1j_0, i_0j_1, i_1j_1) and eight possible transitions between states, each of which reflects the change in configuration of one of the elements (Fig. 1 C). In the absence of any interactions, the transition rates will be given by each element's intrinsic rates γ_i, δ_i, γ_j, and δ_j. When elements i and j interact, each transition rate associated with a change in configuration of element i or j will be

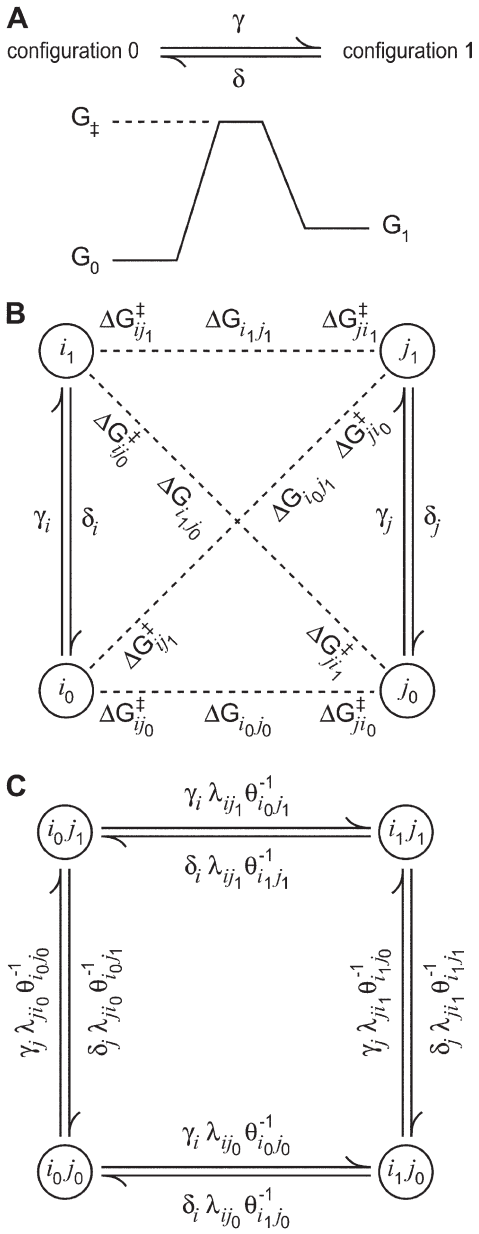

Figure 1. State-dependent interactions between binary elements. (A) Each binary element can transition between its two possible configurations (0 and 1) according to intrinsic rate constants γ and δ, which are defined by the height of a single transition state energy barrier ($G_\ddagger$) in relation to the free energy of each of the elements configurations G_0 and G_1 as defined in Eqs. 1 and 2. (B) An illustration of a pair of binary elements i and j, where each element is represented by a pair of circles for its two possible configurations and its intrinsic transition rates between configurations are shown as arrows. Broken lines indicate the four possible state-dependent interactions for the two elements, each of which is labeled with its three state-dependent interaction energies as described in the Materials and methods. (C) Kinetic scheme represented by the pair of binary elements in B, where each state of the system is shown as a circle labeled with the configurations of each of the elements, and the possible transitions between states reflecting a change in configuration of either of the elements are shown as arrows. Transition arrows are labeled with their rate constants, including all of the possible interaction factors as defined in Eqs. 3–6.

modified according to the interaction's energetic perturbation of both the state from which the transition originates and the transition state intermediate of the element undergoing the change in configuration. For example, the height of the energy barrier governing the transition rate from state i_1j_0 to i_0j_0 will by perturbed by the amount $\Delta G^{\ddagger}_{ij_0} - \Delta G_{i_1 j_0}$. For each element i, adding the appropriate state-dependent interaction energies with every other element j to the free energies of activation in Eqs. 1 and 2 gives the effect of interactions on element i's intrinsic transition rates for any given state of the system as

$$\gamma_i \to \gamma_i \prod_{j \neq i} \frac{\lambda_{ij_q}}{\theta_{i_0 j_q}} \tag{3}$$

$$\delta_i \to \delta_i \prod_{j \neq i} \frac{\lambda_{ij_q}}{\theta_{i_1 j_q}} \tag{4}$$

$$\theta_{i_p j_q} = e^{-\Delta G_{i_p j_q}/k_B T} \tag{5}$$

$$\lambda_{ij_q} = e^{-\Delta G^{\ddagger}_{ij_q}/k_B T}, \tag{6}$$

where the product over j reflects the sum over any number of simultaneous interactions with each other element j; $p \in \{0,1\}$ and $q \in \{0,1\}$ denote the configuration of element i and j, respectively; $\Delta G_{i_p j_q}$ is the interaction energy for those states where elements i and j adopt configurations p and q, respectively; and $\Delta G^{\ddagger}_{ij_q}$ is the energetic perturbation of element i's transition state when element j is in configuration q. The $\theta_{i_p j_q}$ terms reflect the effect of the interaction on the system's metastable states analogous to the equilibrium parameterization used by Chowdhury and Chanda (2010), and the λ_{ij_q} terms reflect the interaction's effect on the transition state intermediates of the interacting elements. Fig. 1 (B and C) illustrates all of the possible state-dependent interaction factors for a two-element system. However, Eqs. 3–6 are valid for an element involved in any number of simultaneous interactions.

As can be seen in Fig. 1 C, traversing around the two-element cyclic state loop for any pair of elements returns the system to the same energy at which it started, and preserves the ratio of the products of transition rates in either direction around the loop. Thus, interactions as defined above maintain microscopic reversibility by construction. This is true for an arbitrary number of binary elements with any number of interactions.

Generalized interactions between elements. In the previous section, the system of binary elements was characterized by specifying the intrinsic transition rates γ_i and δ_i for each element i, and all of the pairwise state-dependent interaction factors $\theta_{i_p j_q}$, λ_{ij_q}, and λ_{ji_p} for each pair of elements i and j. However, this is more information than is required to define the resulting kinetic scheme. That is, the system is "over-parameterized." This can be understood intuitively by considering an element that interacts in both of its configurations, such that it will never behave according to its intrinsic transition rates γ and δ. Indeed, it is often the case experimentally that the behavior of an element in the absence of any interactions is unknown, and it is sufficient to describe only how each element behaves in some reference state of the system, and how this behavior is altered when interaction energies change upon changes in element configuration.

Without loss of generality, we can characterize a system of binary elements using the minimum number of independent parameters by defining two transition rates α_i and β_i for each element i, and three interaction energies ΔG_{ij}, $\Delta G^{\ddagger}_{ij}$, and $\Delta G^{\ddagger}_{ji}$ for each pair of interacting elements i and j. We select the state where all of the elements are in configuration 0 as the zero energy reference state. The rate constants α_i and β_i are the rates at which element i flips configurations when all other elements are in configuration 0 (i.e., the transition rates of each element with respect to the reference state; Fig. 2 A). Thus, α_i and β_i are not necessarily the intrinsic rates γ_i and δ_i; rather, they include all of the interactions between element i and configuration 0 of each other element j as

$$\alpha_i = \gamma_i \prod_{j \neq i} \frac{\lambda_{ij_0}}{\theta_{i_0 j_0}} \tag{7}$$

$$\beta_i = \delta_i \prod_{j \neq i} \frac{\lambda_{ij_0}}{\theta_{i_1 j_0}}. \tag{8}$$

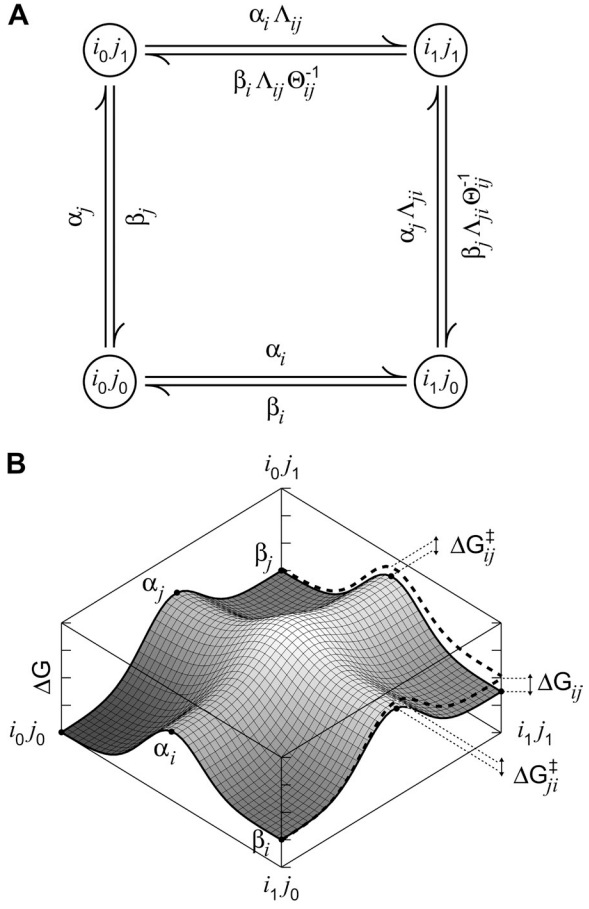

Figure 2. Generalized interactions between binary elements. (A) Kinetic scheme represented by a pair of binary elements i and j, where the transition rates are labeled with the rate constants α and β for each element, and all of the possible generalized interaction factors as defined in Eqs. 7–12. (B) Energy landscape correlate of the kinetic scheme in A, where transitions are only allowed along the edges between states. The i_0j_0 state is set as the zero energy reference state, and the relative energies of the remaining three states and the transition state intermediates between states are labeled with the system parameter that defines them as described in the Materials and methods. Bold broken lines indicate the energy landscape in the absence of any interaction between the elements, the deviation from which is described by the respective allosteric (equilibrium) and catalytic interaction energies.

The interaction energy $\Delta G_{ij}^{\ddagger}$, which imparts a "catalytic" effect, is the difference in the energy barrier governing the transition of element i when element j adopts configuration 1 as compared with configuration 0. $\Delta G_{ji}^{\ddagger}$ is the analogous change for transition of element j when element i adopts configuration 1. Finally, the interaction energy ΔG_{ij}, which imparts the classical "allosteric" effect embodied in the MWC and KNF formulations, is the energy difference between elements i and j both being in configuration 1 as compared with the sum of the energies for either element i or j to be in configuration 1, but not both. These three interaction energies define how the rates α_i and β_i for each element i are perturbed when element j adopts configuration 1 as compared with configuration 0 according to

$$\alpha_i \to \alpha_i \prod_{j \neq i} \Lambda_{ij} \tag{9}$$

$$\beta_i \to \beta_i \prod_{j \neq i} \frac{\Lambda_{ij}}{\Theta_{ij}} \tag{10}$$

$$\Theta_{ij} = e^{-\Delta G_{ij}/k_B T} \tag{11}$$

$$\Lambda_{ij} = e^{-\Delta G_{ij}^{\ddagger}/k_B T}, \tag{12}$$

where the product over j is only over those elements in configuration 1. Fig. 2 A illustrates all of the possible generalized interaction factors for a two-element system. However, Eqs. 9–12 are valid for an element involved in any number of simultaneous interactions. The relationship between the generalized and state-dependent interaction factors for each pair of elements (compare Fig. 1 C and Fig. 2 A) is given by

$$\Theta_{ij} = \frac{\theta_{i_0 j_0} \theta_{i_1 j_1}}{\theta_{i_1 j_0} \theta_{i_0 j_1}} \tag{13}$$

$$\Lambda_{ij} = \frac{\lambda_{ij_1} \theta_{i_0 j_0}}{\lambda_{ij_0} \theta_{i_0 j_1}} \tag{14}$$

$$\Delta G_{ij} = \left(\Delta G_{i_0 j_0} + \Delta G_{i_1 j_1}\right) - \left(\Delta G_{i_1 j_0} + \Delta G_{i_0 j_1}\right) \tag{15}$$

$$\Delta G_{ij}^{\ddagger} = \left(\Delta G_{ij_1}^{\ddagger} - \Delta G_{i_0 j_1}\right) - \left(\Delta G_{ij_0}^{\ddagger} - \Delta G_{i_0 j_0}\right). \tag{16}$$

Fig. 2 B illustrates the energy landscape correlate of the kinetic scheme for a pair of interacting elements i and j as depicted in Fig. 2 A. It is clear that the eight transition rates are completely defined by the relative energies between the four possible states and four transition state barriers between states, where we take the energy of the $i_0 j_0$ state as our zero energy reference. The parameters α_i, β_i, α_j, and β_j define the relative energies of the $i_1 j_0$ and $i_0 j_1$ states as well as the transition state barriers between them and the $i_0 j_0$ state. The transition state barriers between the $i_1 j_0$ and $i_0 j_1$ states and the $i_1 j_1$ state are defined relative to the first two transition state barriers by the interaction energies $\Delta G_{ij}^{\ddagger}$ and $\Delta G_{ji}^{\ddagger}$, and ΔG_{ij} sets the energy of the $i_1 j_1$ state relative to the sum of the energies of the $i_1 j_0$ and $i_0 j_1$ states. This is analogous to defining seven of the eight transition rates, where the eighth rate is constrained by microscopic reversibility (Colquhoun et al., 2004).

For a system of N binary elements, there are

$$\sum_{k=1}^{N-1} k = N(N-1)/2$$

possible pairs of interacting elements, and the maximum number of system parameters $n_{\text{dof-max}}$ accounts for two transition rates per element and three interaction energies per pair of elements according to

$$n_{dof-max} = 2N + 3N(N-1)/2. \tag{17}$$

Computing the transition rates between system states. All of the transition rates between system states are defined by Eqs. 7–12. For a system of N elements, there will be 2^N states, but only N allowed transitions into or out of each state corresponding to the change in configuration of one of the elements (i.e., transitions between states that differ in the configuration of more than one element are disallowed; see Fig. 3). Each system state can be represented by a unique 0-based integer index $\in [0, 2^N - 1]$ corresponding to the binary representation of each of the elements (Fig. 3 A). For example, "101" is denoted by the index 5 and represents the state of a three element system where the first and third elements are in configuration 1 and the second element is in configuration 0. For a transition from state index u to state index v, the index i of the single element undergoing a change in configuration between states u and v satisfies $(1 << i) = (u \wedge v)$, where << and ^ are the bitwise shift and exclusive OR operators, respectively. Furthermore, if $(1 << i) \,\&\, u = 0$, then element i transitioned from configuration 0 to configuration 1, otherwise vice versa, where & is the bitwise AND operator. For example, consider the transition from "101" ($u = 5$) to "111" ($v = 7$). In this case, the element having the 0-based index $i = 1$ flipped from configuration 0 to 1, and it holds that $(1 << 1) = (5 \wedge 7)$ and $(1 << 1) \,\&\, 5 = 0$. Therefore, the transition rate k_{uv} from state u to state v is given by

$$k_{uv} = \begin{cases} \alpha_i \prod_{j \neq i} \Lambda_{ij} & \text{if } (1 \ll i) = (u \wedge v) \text{ and } (1 \ll i) \,\&\, u = 0 \\ \beta_i \prod_{j \neq i} \frac{\Lambda_{ij}}{\Theta_{ij}} & \text{if } (1 \ll i) = (u \wedge v) \text{ and } (1 \ll i) \,\&\, u = 1 \\ 0 & \text{otherwise} \end{cases}, \tag{18}$$

where i is the index of the element changing configurations, the product over element indices j is over only those elements that are both in configuration 1 (i.e., $(1 << j) \,\&\, u = 1$) and are interacting with the element having index i, and the rate constants and interaction factors refer to Eqs. 7–12.

$GABA_A$ receptor kinetic models

Channels were modeled as collections of interacting "binary elements" as described above. All model parameters are referenced with respect to the symbol of their associated elements such that α_i and β_i are the rate constants for element i, and Θ_{ij}, Λ_{ij}, and Λ_{ji} are the interaction factors between elements i and j (see Eqs. 7–12). The sets of differential equations describing the time-dependent probability of state occupancies are defined by the transition rates between states as given in Eq. 18, and were solved numerically, either using an eigensystem decomposition of the matrix of transition rates (Colquhoun and Hawkes, 1995), a fourth order Runge-Kutta differential equation solver with error checking and adaptive step sizes (Press et al., 2007), or by Monte Carlo

techniques. Programs were written in C++ (see "Availability of software" below).

For each of schemes I–III (Fig. 4 A), the agonist binding sites were coupled directly to the main gate, such that bound agonist speeds main gate opening by the factor Λ_{mA}. For simplicity, we set $\Lambda_{mA} = \Theta_{Am}$ and $\Lambda_{Am} = 1$, which results in no net change to the main gate closing rate upon agonist binding. The main gate closing rate β_m was set to 380 s^{-1} based on observed single channel open times (Keramidas and Harrison, 2008), and the opening rate α_m was constrained according to $\alpha_m = \beta_m P_{o\text{-}min}/(1 - P_{o\text{-}min})$, where $P_{o\text{-}min} = 1e^{-5}$ is the channel's estimated spontaneous opening probability (Campo-Soria et al., 2006). Finally, the interaction energy between each agonist binding site and the main gate was obtained from the constraint $\Lambda_{mA}{}^2\alpha_m = \beta_m P_{o\text{-}max}/(1 - P_{o\text{-}max})$, where $P_{o\text{-}max} = 0.8$ is the single channel intraburst open probability in the presence of saturating GABA (Keramidas and Harrison, 2010). Thus, $\Lambda_{mA} = \Theta_{Am} = 632$, which at a temperature of 298.15 K corresponds to $\Delta G_{Am} = -3.8$ kcal/mol.

We coupled the agonist binding sites directly to either one or both desensitization gates in an analogous fashion to the main gate (i.e., $\Lambda_{dA} = \Theta_{Ad}$ and $\Lambda_{Ad} = 1$, where d represents either d_f or d_s). Fits to our experimental data were most sensitive to the combination of desensitization gate transition rates and their energetic coupling, rather than either one of these parameters alone. Thus, we arbitrarily fixed the energy of each interaction with the desensitization gates, and only allowed the rates of desensitization/resensitization to vary. For scheme I, we set $\Theta_{Ad_f} = \Theta_{Ad_s} = 10$, which corresponds to $\Delta G_{Ad_f} = \Delta G_{Ad_s} = -1.4$ kcal/mol. For schemes II and III, we set $\Theta_{Ad_s} = 7.26$ and $\Theta_{Ad_f} = 7.26$, respectively, for a net agonist binding energy of $\Delta G_{Am} + \Delta G_{Ad} = -5$ kcal/mol (d represents either d_f or d_s), similar to observations of the thermodynamics of ligand binding (Jackson, 1993; Maksay, 1994).

The drug unbinding rate in schemes IV–VI (Fig. 5, A and C; and Fig. 6 A) was set to $\beta_D = 0.3$ s^{-1} based on measurements of the kinetics of diazepam unbinding (Goldschen-Ohm et al., 2010), and the binding rate was estimated as $\alpha_D = \beta_D/K_D = 1 \times 10^8$ $M^{-1}s^{-1}$, where K_D is the affinity constant found in radioligand binding and current potentiation experiments (Sieghart, 1995; Boileau et al., 1998). For scheme VI, the interactions between the intermediate elements and the main and desensitization gates is analogous to those between the agonist binding sites and channel gates in scheme I (i.e., $\Theta_{mF} = \Theta_{mA}$ and $\Theta_{dF} = \Theta_{dA}$, where d represents either d_f or d_s). The direct interaction with each agonist binding site was constrained such that $\Theta_{AF} = 4{,}590$, which corresponds to $\Delta G_{AF} = -5$ kcal/mol at 298.15 K similar to observations of the free energy of GABA binding (Maksay, 1994). For simplicity, one of the two catalytic interaction factors was further constrained by requiring that $\Theta_{AF} = \Lambda_{AF}\Lambda_{FA}$ with $\Lambda_{AF} \in [1,\Theta_{AF}]$, which is equivalent to splitting the interaction energy ΔG_{AF} between each of the interacting element's transition state intermediates (i.e., $\Delta G_{AF} = \Delta G^{\ddagger}_{AF} + \Delta G^{\ddagger}_{FA}$). The drug-binding site in scheme VI was coupled to one of the intermediate elements in an analogous fashion to agonist binding (i.e., $\Theta_{DF} = \Lambda_{DF}\Lambda_{FD}$), although the interaction energy Θ_{DF} was allowed to vary.

Models were optimized by minimizing the weighted sum of squared errors between simulated and observed $GABA_A$ receptor currents in response to rapid application of GABA onto outside-out patches from HEK 293 cells expressing human $\alpha_1\beta_2\gamma_2$ receptors (solution exchange <200 µs for accurate measurement of fast receptor kinetics; see "Patch clamp electrophysiology" above). Time points were weighted according to a decaying exponential plus a constant for each period of constant stimulus, such that time points immediately after a change in stimuli (e.g., application of GABA) where currents are changing most rapidly are given the most weight. Current responses to saturating (10 mM) GABA were scaled to a peak open probability of 0.7 based on noise analysis (Goldschen-Ohm et al., 2010), and current responses to 30 µM GABA were scaled based on the relative peak current between interleaved 10 mM and 30 µM GABA pulses for individual patches (see Fig. 4 C). Current responses to 30 µM GABA were scaled based on preliminary model simulations after fitting to 10 mM and 30 µM GABA responses. Optimization involved simultaneously fitting exemplary $GABA_A$ receptor current responses to multiple stimulus protocols, a stringent constraint designed to ensure that the models can describe numerous aspects of channel behavior. Current recordings from a minimum of three separate patches were used for each stimulus protocol.

Availability of software

The software used to simulate and optimize the kinetic models are available as Supplemental material. To get the latest version of the software, we recommend checking for future updates that may be available at http://www.sourceforge.net/projects/modbuilder. The software includes a graphical interface for constructing new models and simulating their activity in response to user-defined stimuli.

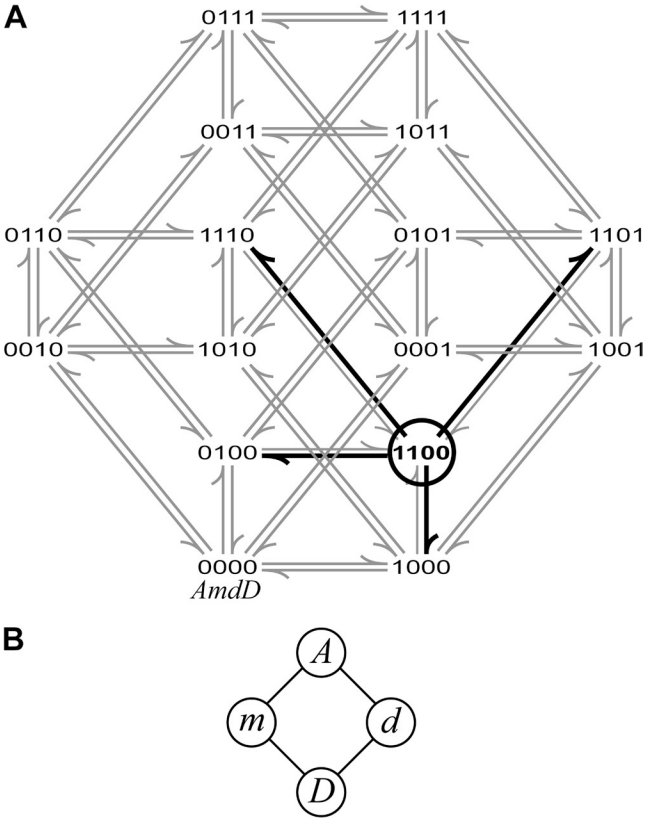

Figure 3. Binary elements model representation. (A) A standard representation of a four element kinetic scheme composed of an agonist-binding site (A), a main gate (m), a desensitization gate (d), and a drug-binding site (D). States are labeled by the bit-wise representation of the element configurations (i.e., "0100" represents the state $A_0m_1d_0D_0$). Although the model contains 16 states, there are only four transitions into or out of any given state (e.g., circled state and bold transition arrows). (B) A binary elements representation of the same model shown in A, where each element is depicted as a labeled circle and interacting elements are connected by solid lines. This representation is analogous to that used previously to describe systems of linked particles (e.g., Sigg, 2013). Note that not all possible interactions are labeled (e.g., binding sites interact with gates, but not each other).

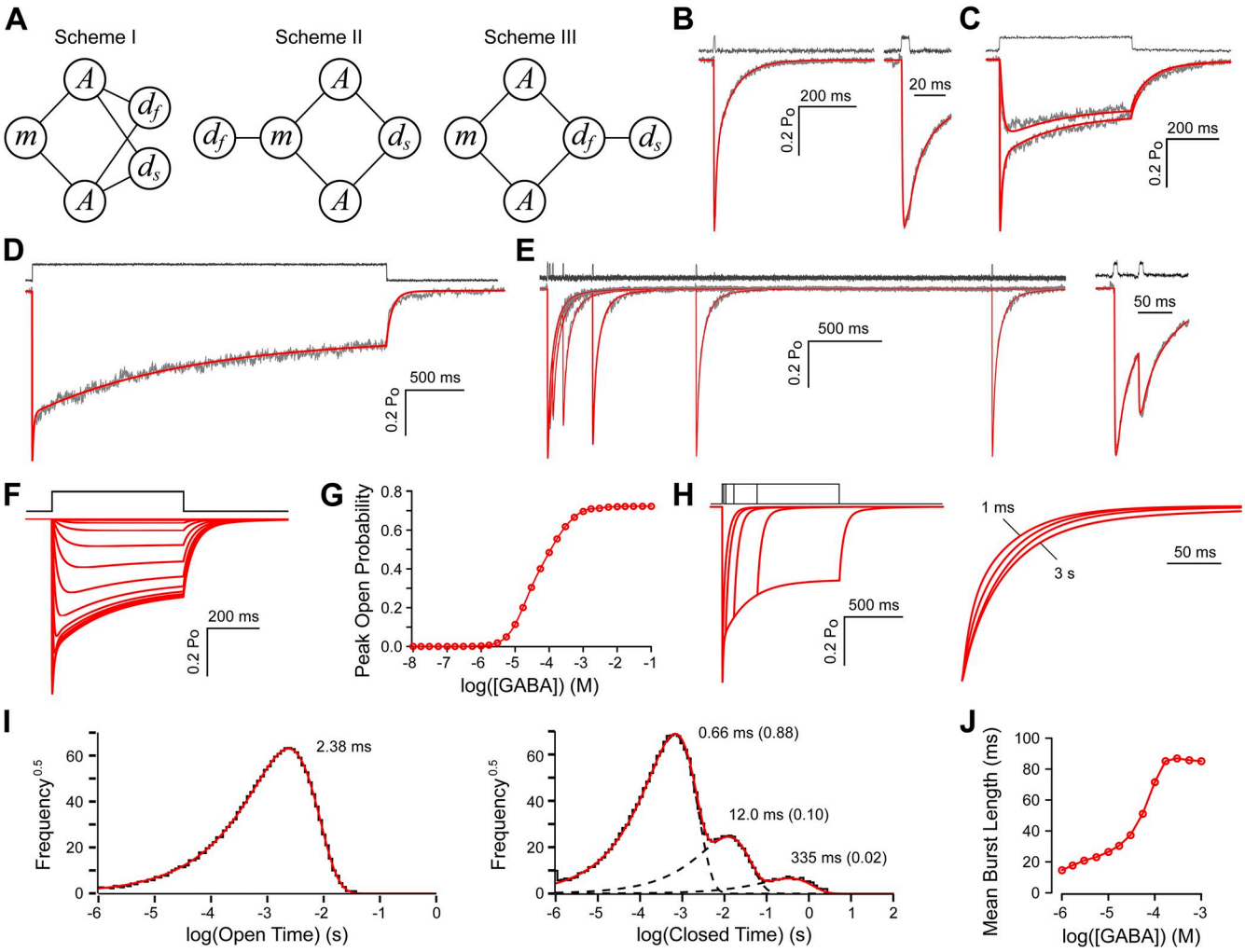

Figure 4. An elements-based kinetic model of the $GABA_A$ receptor. (A) Three binary elements model representations for the $GABA_A$ receptor (schemes I–III) incorporating two agonist binding sites A that are either unoccupied (A_0) or occupied (A_1), each of which interacts with a main channel gate m and fast and slow desensitization gates d_f and d_s that are either closed (m_0, d_{f1}, d_{s1}) or open (m_1, d_{f0}, d_{s0}). The channel is conducting when all three gates are open. Elements are depicted as labeled circles, and interactions as lines connecting the pair of interacting elements (e.g., see Fig. 3). All model parameters are referenced with respect to the symbol of their associated elements such that α_i and β_i are the rate constants for element i, and Θ_{ij}, Λ_{ij}, and Λ_{ji} are the interaction factors between elements i and j (see Materials and methods and Eqs. 7–12). Model parameters reflect simulations at a temperature of 298.15 K. Optimized rate constants ($[M^{-1}]s^{-1}$) across patches for scheme I: $\alpha_A = 2.3 \pm 0.2 \times 10^6$, $\beta_A = 91 \pm 9$, $\alpha_{df} = 0.40 \pm 0.03$, $\beta_{df} = 86 \pm 9$, $\alpha_{ds} = 0.021 \pm 0.008$, $\beta_{ds} = 2.6 \pm 0.9$. For scheme II: $\alpha_A = 1.9 \pm 0.2 \times 10^6$, $\beta_A = 86 \pm 4$, $\alpha_{df} = 0.50 \pm 0.04$, $\beta_{df} = 82 \pm 7$, $\alpha_{ds} = 0.020 \pm 0.005$, $\beta_{ds} = 1.2 \pm 0.5$. For scheme III: $\alpha_A = 2.0 \pm 0.2 \times 10^6$, $\beta_A = 81 \pm 6$, $\alpha_{df} = 0.65 \pm 0.07$, $\beta_{df} = 62 \pm 6$, $\alpha_{ds} = 0.027 \pm 0.006$, $\beta_{ds} = 1.3 \pm 0.5$. All other model parameters were constrained as described in the Materials and methods. (B–E) Simulated open probability (red) overlaid on an outside-out patch current recording (gray) in response to rapid application of GABA (top trace is the solution exchange time course at the pipet tip after the experiment; see Materials and methods). Simulations in B–J are shown for scheme I, although nearly indistinguishable simulations were obtained for schemes II and III. (B) Simulated and observed current response to a 4-ms pulse of 10 mM GABA. The same responses are shown to the right on an expanded time scale. (C) Simulated and observed current response to a 500-ms pulse of either 30 µM or 10 mM GABA (pulses were interleaved on the same patch). (D) Simulated and observed current response to a 3-s pulse of 10 mM GABA. (E) Simulated and observed current responses to pairs of 5-ms pulses of 10 mM GABA separated by a variable recovery period (responses to six separate pulse pairs for a single patch are shown overlaid). One of the pulse pairs is shown to the right on an expanded time scale. (F) Simulated responses to a family of 500-ms pulses of varying GABA concentrations from 10 nM to 100 mM. (G) Peak current dose–response relationship for the simulated currents in *F*. The median ligand concentration (see Chowdhury and Chanda, 2013) was 50.3 µM GABA. (H) Simulated responses to varying duration pulses of 10 mM GABA (left, individual responses overlaid) illustrate the prolongation of deactivation by desensitization (right, deactivation after 1 ms–3 s pulses of 10 mM GABA are aligned to their onset and normalized). (I) Open and closed dwell time histograms from Monte Carlo simulations of a single channel in 10 mM GABA. Exponential time constants (and relative areas) from maximum likelihood fits (solid red) to the dwell time distributions (solid black) are labeled (individual exponential components of the fit are shown as broken black lines). (J) Agonist dependence of single channel burst lengths separated by closures longer than 15 ms.

Online supplemental material

The code for the software used to simulate and optimize the kinetic models is provided, as well as a user's guide and a Mac OS X disk image for simple drag-and-drop installation. Online supplemental material is available at http://www.jgp.org/cgi/content/full/jgp.201411183/DC1.

RESULTS

An elements-based kinetic model of the $GABA_A$ receptor

We constructed a simple $GABA_A$ receptor model incorporating two agonist binding site elements (A), a main gate (m), and fast and slow desensitization gates (d_f, d_s), such that all three gates (m, d_f, d_s) must be open for the channel to conduct current. We explored three different sets of interactions between these elements in which at rest the main and desensitization gates are closed and open, respectively, and agonist binding promotes main gate opening and desensitization gate closing for a desensitizing current response (Fig. 4 A, schemes I–III). Schemes I–III each have $2^5 = 32$ states, but assuming equivalent agonist binding sites and applying several constraints based on observations of single channels and agonist binding thermodynamics (see Materials and methods) yields a total of only six free parameters describing the transition rates of agonist binding/unbinding and opening/closing of each desensitization gate. The models were optimized by fitting to observed $GABA_A$ receptor currents in response to rapid application of GABA onto outside-out patches from HEK 293 cells expressing human $\alpha_1\beta_2\gamma_2$ receptors (solution exchange <200 µs for accurate measurement of fast receptor kinetics; see Materials and methods). The final model parameters across patches (mean ± SEM) are given in the legend for Fig. 4.

Each of schemes I–III was able to quantitatively account for all of the stimulus protocols shown in Fig. 4, with nearly indistinguishable fits to the observed current time courses. Fig. 4 B illustrates both simulated and observed $GABA_A$ receptor currents in response to a brief 4-ms pulse of 10 mM GABA, similar to the stimulus conditions at a synapse. During prolonged 500-ms and 3-s pulses of 10 mM GABA at least two kinetic components of desensitization become apparent (Fig. 4, C and D, respectively), which are accounted for in schemes I–III by the fast and slow desensitization gates. The time course of recovery from desensitization was assayed with pairs of 5-ms pulses of 10 mM GABA separated by a variable recovery period (Fig. 4 E). Finally, the agonist concentration dependence of the kinetics of both activation and desensitization was estimated by measuring the peak response to 500-ms pulses of both saturating 10 mM and subsaturating 30 µM GABA in the same patch (Fig. 4 C; 10 mM and 30 µM pulses were interleaved).

A family of simulated responses to 500-ms pulses of 10 nM–100 mM GABA are shown in Fig. 4 F, which describes a peak dose–response relationship with a median ligand concentration of 50.3 µM GABA (Fig. 4 G; see Chowdhury and Chanda [2013] for a description of median ligand concentration). Although the constraint on the dose–response relationship is largely caused by the relative kinetics and peak responses elicited by 10 mM versus 30 µM GABA, the resulting model prediction is consistent with previous observations of the concentration dependence of peak currents in response to rapid application of GABA (<200 µs solution exchange time) over a larger concentration range (e.g., Mozrzymas et al., 2003). Model simulations also predict that increased desensitization during prolonged GABA application results in the prolongation of deactivation after GABA removal, as observed in $GABA_A$ receptors studied using rapid solution exchange methods (Fig. 4 H; Jones and Westbrook, 1995).

Despite having 32 states, open and closed dwell time distributions from Monte Carlo simulations had small numbers of components: one open and three closed (Fig. 4 I). In the presence of a saturating concentration of GABA (10 mM), thereby simulating a "cluster analysis" type of experiment (Keramidas and Harrison, 2008), the single apparent open state was largely governed by the main gate closing rate ($\beta_m^{-1} = 2.6$ ms), whereas the three apparent closed states reflected the opening rates of the main and desensitization gates in the presence of two bound agonists ($((\alpha_m\Lambda_{ma}^2)^{-1} = 0.66$ ms; $\beta_{d_f}^{-1} = 11.6$ ms; $\beta_{d_s}^{-1} = 391$ ms). Burst lengths separated by closures longer than 15 ms were concentration dependent (Fig. 4 J) similar to observations in single channel records (Keramidas and Harrison, 2010).

Drug modulation of binding versus gating

Although numerous clinically important drugs exert their effects by modulating ligand-gated ion channels (Kaczorowski et al., 2008), it is often unclear whether these drugs function by altering channel gating or agonist binding, both of which contribute to shaping postsynaptic current kinetics. In general, relating drug effects on observed physiological responses to modulation of receptor microscopic properties depends on the structure of the kinetic model used. Thus, we explored the predicted effects of drug binding in scheme I (Fig. 4 A) for either modulation of the main gate (Fig. 5 A, scheme IV) or an agonist binding site (Fig. 5 C, scheme V). In scheme IV, the drug binding site (D) was coupled to the main gate analogous to an agonist binding site, albeit with different energetics. In scheme V, drug binding directly affected the agonist binding rate and the stability of the bound agonist. See the legend for Fig. 5 for parameter values.

Drug binding in both schemes IV and V had nearly identical effects on receptor kinetics, slowing deactivation without altering desensitization (Fig. 5, B and D). However, drug binding in schemes IV and V had different effects on the channel's peak dose–response relationship (Fig. 5 E),

knowledge of which can potentially discriminate between the two schemes (Wagner et al., 2004; Goldschen-Ohm et al., 2011). Although peak dose–response curves were left-shifted in the presence of drug for both schemes IV and V, only for scheme IV did drug binding increase the peak open probability in the presence of saturating GABA. Also, only scheme IV allows for drug binding to promote channel activation in the absence of agonist (i.e., increase the resting state open probability).

An elements-based kinetic model for BZD-positive modulation of $GABA_A$ receptors

BZDs are an important class of $GABA_A$ receptor modulators that bind at an interface between subunits (Pritchett et al., 1989; Wieland et al., 1992; Boileau and Czajkowski, 1999). They are used in clinical practice for procedural sedation and to treat a wide variety of conditions including disorders of mood and anxiety, epilepsy, and many others (Rudolph and Knoflach, 2011). However, their kinetic effects on the channel remain a matter of contention, with multiple studies reporting nearly exclusive changes in either binding (Vicini et al., 1987; Rogers et al., 1994; Lavoie and Twyman, 1996; Mellor and Randall, 1997; Perrais and Ropert, 1999; Goldschen-Ohm et al., 2010) or gating (Downing et al., 2005; Rüsch and Forman, 2005; Campo-Soria et al., 2006; Gielen et al., 2012; Li et al., 2013), the totality of which cannot be explained by either scheme IV (Fig. 5 A) or V (Fig. 5 C). For example, scheme IV predicts that drug binding will increase the peak open probability in response to a saturating agonist, whereas BZDs do not potentiate responses to saturating GABA. In contrast, drug binding in scheme V will not enhance the peak open probability at a saturating concentration of either a full or partial agonist, whereas BZDs can potentiate the peak open probability in response to saturating partial agonists, as opposed to full agonists.

To reconcile these seemingly disparate observations, we extended scheme I (Fig. 4 A) to allow both GABA and BZD-positive modulator binding to similarly influence the configuration of an intermediate element involved in transducing ligand binding to channel gating, although with different energetics for GABA versus BZDs (Fig. 6 A, scheme VI). Here, the ligand-binding sites and channel gates do not directly interact, but instead ligand binding promotes activation of an intermediate transduction element (*F*), which is coupled to the main and desensitization gates analogously to how the agonist-binding sites were so coupled in scheme I (Fig. 4 A). We treat BZD-positive modulator binding at the drug-binding site element (*D*) in an analogous fashion to agonist binding, albeit with a different energy. Scheme VI has $2^8 = 256$ states, but applying the same constraints used for scheme I and constraining the agonist binding energy at 298.15 K to $\Delta G_{AF} = -5$ kcal/mol, similar to observations for the thermodynamics of GABA binding (Maksay, 1994), yields only 11 free parameters (see Materials and methods). The final optimized model parameters based on fits to observed $GABA_A$ receptor currents in response to rapid application of GABA (solution exchange <200 µs; see Materials and methods) across patches (mean ± SEM) are given in the legend for Fig. 6.

Drug binding in scheme VI stabilizes one of the intermediate elements in its activated configuration, thus

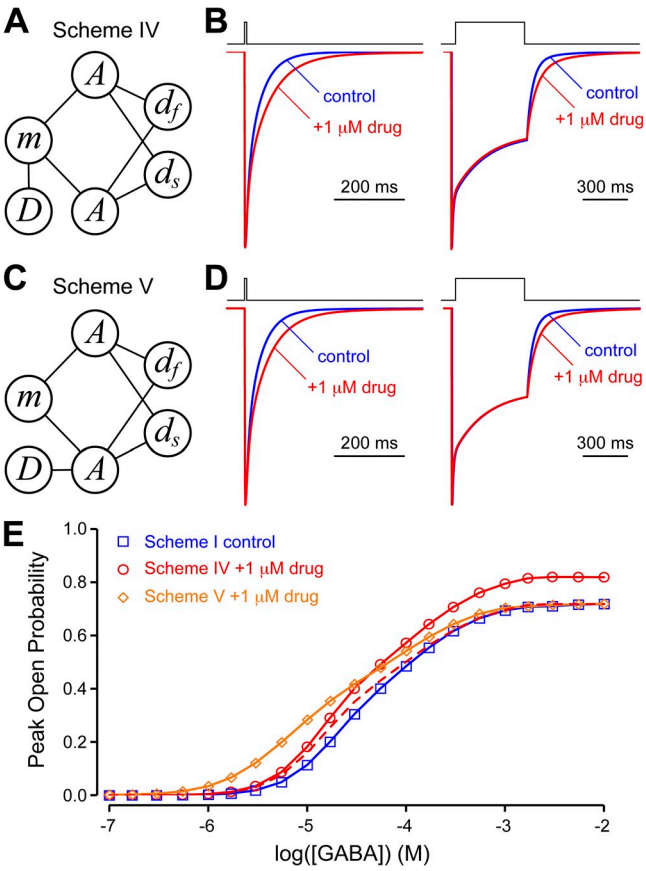

Figure 5. Predictions for drugs that modulate channel gating versus agonist binding. (A and C) A drug binding element (*D*) was added to scheme I (Fig. 4 A) such that it interacts with either the main gate (scheme IV) or one of the agonist binding sites (scheme V). Elements are depicted as labeled circles, and interactions as lines connecting the pair of interacting elements (e.g., see Fig. 3). All model parameters are referenced with respect to the symbol of their associated elements such that α_i and β_i are the rate constants for element *i*, and Θ_{ij}, Λ_{ij}, and Λ_{ji} are the interaction factors between elements *i* and *j* (see Materials and methods and Eqs. 7–12). Model parameters for schemes IV and V are as described for scheme I, and drug binding/unbinding rates were set to $\alpha_D = 1 \times 10^8\ M^{-1}s^{-1}$ and $\beta_D = 0.3\ s^{-1}$, as described in the Materials and methods. Drug-bound interaction factors for scheme IV: $\Theta_{Dm} = 2$, $\Lambda_{mD} = 2$, $\Lambda_{Dm} = 1$. For scheme V: $\Theta_{DA} = 25$, $\Lambda_{AD} = 5$, $\Lambda_{DA} = 5$. (B and D) Simulated normalized current responses to 4-ms (left) or 500-ms (right) pulses of 10 mM GABA in the absence (control) or presence of 1 µM drug for scheme IV (B) and scheme V (D). (E) Simulated peak open probability dose–response relationship for schemes I, IV, and V. The broken line depicts scheme IV normalized to the maximal peak open probability for scheme I.

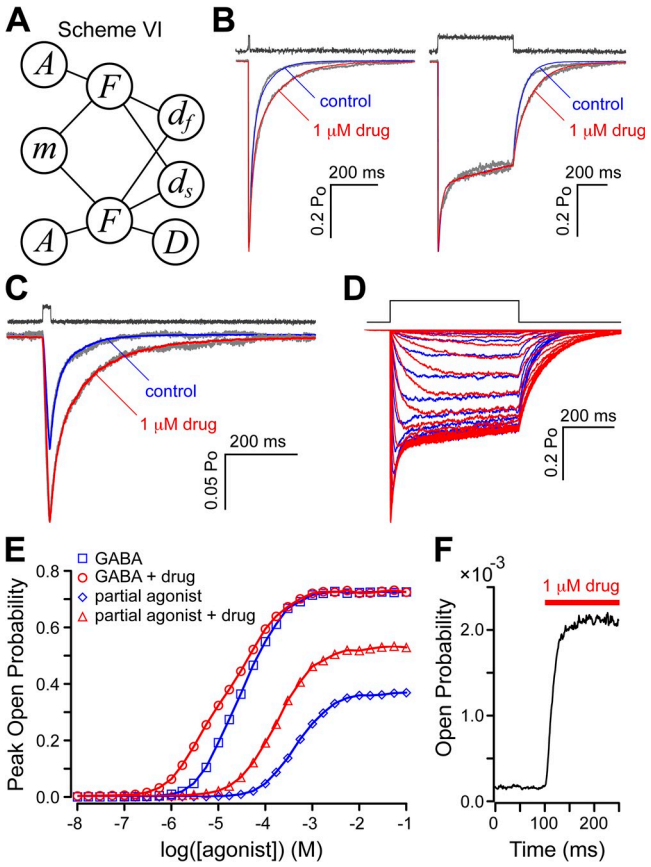

Figure 6. An elements-based kinetic model for BZD-positive modulation of $GABA_A$ receptors. (A) Binary elements model representation, which extends scheme I (Fig. 4 A) by inserting intermediate elements (F) involved in transducing agonist binding at two agonist binding site elements (A) to gating of both main and fast/slow desensitization gates (m, d_f, d_s). In addition, a drug-binding site (D) is coupled to one of the intermediate elements. Elements are depicted as labeled circles, and interactions as lines connecting the pair of interacting elements (e.g., see Fig. 3). All model parameters are referenced with respect to the symbol of their associated elements such that α_i and β_i are the rate constants for element i, and Θ_{ij}, Λ_{ij}, and Λ_{ji} are the interaction factors between elements i and j (see Materials and methods and Eqs. 7–12). Model parameters reflect simulations at a temperature of 298.15 K. Optimized rate constants ($[M^{-1}]s^{-1}$) across patches are $\alpha_A = 3.2 \pm 0.1 \times 10^6$, $\beta_A = 1{,}836 \pm 124$, $\alpha_F = 5.5 \pm 0.4$, $\beta_F = 1124 \pm 25$, $\alpha_{df} = 0.25 \pm 0.02$, $\beta_{df} = 31 \pm 2$, $\alpha_{ds} = 3.3 \pm 0.3 \times 10^{-3}$, and $\beta_{ds} = 0.19 \pm 0.01$. Optimized interaction factors are $\Lambda_{FA} = 3{,}191 \pm 25$, $\Theta_{DF} = 18.6 \pm 1.1$, and $\Lambda_{DF} = 2.6 \pm 0.1$. All other model parameters were constrained as described in the Materials and methods. (B) Simulated open probability in response to 4-ms (left) or 500-ms (right) pulses of 10 mM GABA either in the absence (control) or presence of 1 μM of drug for scheme VI, overlaid on current recordings from outside-out patches (gray). Current recordings in the presence and absence of 1 μM of the BZD-positive modulator diazepam (DZ) were interleaved on the same patch. The top trace is the solution exchange time course at the pipet tip after the experiment (see Materials and methods). (C) Same as B, except for 20-ms pulses of 10 μM GABA. (D) Family of simulated current responses to 500-ms pulses of varying GABA concentrations in the absence (blue traces) or presence of 1 μM drug (red traces). (E) Peak open probability dose–response relationships for both full (e.g., GABA) and partial agonists in the absence and presence of 1 μM drug. Partial agonism was modeled by a reduced interaction energy between agonist-binding sites and the intermediate elements (see Results). (F) Increase in simulated unliganded channel open probability upon application of 1 μM drug (red bar) for scheme VI.

slowing deactivation kinetics as observed in the presence of 1 μM of the BZD-positive modulator diazepam after both brief (4 ms) and prolonged (500 ms) pulses of saturating (10 mM) GABA (Fig. 6 B), similar to observations for inhibitory postsynaptic currents (IPSCs; Mellor and Randall, 1997; Perrais and Ropert, 1999). As observed during 500-ms pulses of 10 mM GABA, desensitization is not affected by bound drug (Fig. 6 B, right). Consistent with previous reports, diazepam potentiated peak current responses to rapid application of subsaturating GABA (10 μM; Fig. 6 C), but not saturating GABA (10 mM; Fig. 6 B), observations that were previously interpreted to suggest predominant changes in binding only (Lavoie and Twyman, 1996; Mellor and Randall, 1997; Perrais and Ropert, 1999; Goldschen-Ohm et al., 2010). In scheme VI (Fig. 6 A), this reflects the relatively much greater ability of bound GABA to activate its associated intermediate element than bound drug ($\Delta G_{DF} = -1.7$ kcal/mol at 298.15 K), such that drug binding while GABA is bound provides very little additional enhancement of current activation. In contrast, for subsaturating GABA concentrations drug binding allosterically promotes GABA binding at unoccupied GABA binding sites (and stabilizes GABA once bound) via its stabilization of the activated intermediate element. The simulated peak open probability dose–response relationship was left shifted from a median ligand concentration of 30.8 μM to 14.7 μM GABA in the presence of 1 μM drug (Fig. 6, D and E), similar to previous observations of the concentration dependence of BZD potentiation (Downing et al., 2005; Campo-Soria et al., 2006; Gielen et al., 2012; Li et al., 2013).

Drug binding in scheme VI can also account for the observation that BZD-positive modulators increase the efficacy of partial, but not full agonists (e.g., GABA; Fig. 6 E; Downing et al., 2005; Rüsch and Forman, 2005; Campo-Soria et al., 2006; Gielen et al., 2012; Li et al., 2013). Here, partial agonism was modeled by decreasing the interaction energy between the agonist binding sites and intermediate elements to $\Delta G_{AF} = -3$ kcal/mol at 298.15 K, although similar effects could be obtained by a combination of reductions in binding energy ΔG_{AF} and binding rate α_A. In scheme VI (Fig. 6 A), the drug-enhanced efficacy of partial agonists reflects the decreased disparity between drug and agonist binding on activation of the intermediate element. Scheme VI (Fig. 6 A) also allows for drug binding to influence the channel opening probability in the absence of bound agonist by directly promoting activation of the associated intermediate element (Fig. 6 F), observations

previously ascribed to exclusive effects on channel gating (Downing et al., 2005; Rüsch and Forman, 2005; Campo-Soria et al., 2006; Gielen et al., 2012). Thus, the major observations for BZD-positive modulation of $GABA_A$ receptors including detailed kinetics, direct gating, and enhanced efficacy of partial agonists can be explained by positing that BZD-positive modulators themselves act as weak partial agonists whose effects on downstream gating elements are additive to those of agonist binding at one of the two agonist-binding sites.

DISCUSSION

The models shown in Figs. 4 A and 6 A reproduce many aspects of both equilibrium and nonequilibrium $GABA_A$ receptor behavior. In addition, scheme VI (Fig. 6 A) accounts for the effects of drug modulation by BZD-positive modulators on both the detailed kinetics of receptor behavior in response to multiple stimulus protocols, as well as dose–response relationships for both full and partial agonists, and also allows drug binding to itself modulate the open/closed equilibrium as observed in spontaneously open mutants. Despite having 256 states, by postulating a model "structure" based upon our intuition of how the elements interact with each other, and applying experimental constraints on both the rate constants and interaction energies as described, we are left with only 11 free parameters. This compares favorably with other kinetic models of $GABA_A$ receptor gating, most of which incorporate between 10 and 24 parameters and do not include drug binding or modulation (Jones and Westbrook, 1995; Haas and Macdonald, 1999). However, our models remain oversimplified. For example, single channel recordings exhibit more open/closed states than are apparent in our simulated dwell time distributions, and also show a redistribution of channel openings among observed open states across agonist concentrations (Haas and Macdonald, 1999; Keramidas and Harrison, 2008). Nonetheless, schemes I–III provide a starting point for more complicated models such as scheme VI, which provides an intuitive mechanistic description of drug modulation that can explain the kinetic changes underlying drug action at synapses.

BZD-positive modulation of $GABA_A$ receptors

Neither direct modulation of either the main gate or one of the agonist binding sites was alone sufficient to explain the totality of observations for BZD-positive modulators (Fig. 5, schemes IV and V). In contrast, allowing drug binding to modulate an intermediate element involved in transducing ligand binding to channel gating accounts for both equilibrium and nonequilibrium observations for BZD-positive modulators, including all of the effects previously ascribed to exclusive changes in either binding or gating (Fig. 6 A, scheme VI). Scheme VI posits a direct interaction between the drug-binding site and only one of the two intermediate transduction elements based on the proximity of BZD and GABA binding sites in a structural model (Bergmann et al., 2013). Interestingly, a similar conclusion that BZDs directly modulate only one of the two GABA binding events was reached based on single channel observations (Macdonald and Olsen, 1994).

The inclusion of an intermediate element between agonist binding and channel gating builds upon a previous model proposed by Gielen et al. (2012), hereafter referred to as the GLS model, where BZDs influence a preactivation step intermediate to ligand binding and channel gating. There are several significant enhancements and important differences between scheme VI and the GLS model. First, the GLS model was parameterized for equilibrium conditions only, whereas scheme VI describes both the equilibrium and nonequilibrium kinetic effects of BZD-positive modulators. Second, the GLS model, like the allosteric schemes on which it was based (Downing et al., 2005; Rüsch and Forman, 2005; Campo-Soria et al., 2006), does not consider desensitization, a potentially confounding complication when comparing model simulations to peak current observations, which are shaped by both activation and desensitization processes. Third, for scheme VI, BZD-positive modulator binding affects both agonist binding and gating via the propagation of interactions from the BZD binding site to both the agonist-binding site and channel gates. In contrast, BZD binding in the GLS model does not affect the agonist-binding step itself, but only a subsequent gating step. Because peak current is a nonequilibrium measure depending on both binding and gating, additional evidence such as a measure of binding alone is necessary to distinguish between these two model predictions. Finally, the GLS model postulates different sets of gating equilibrium constants for agonists versus partial agonists, whereas scheme VI provides an explanation based exclusively on differences in interactions between ligands and their binding sites.

Scheme VI (Fig. 6 A) predicts that GABA binding should reciprocally stabilize BZD-positive modulator binding via the stabilization of the activated intermediate transduction element. Such reciprocal interactions between the BZD and GABA binding sites have been observed, as changes in the rates of accessibility of an introduced cysteine residue to methanethiosulfonate reagents at either the GABA or BZD binding site upon ligand binding at the other site (Kloda and Czajkowski, 2007; Sharkey and Czajkowski, 2008).

In summary, we provide a $GABA_A$ receptor model that describes both the detailed kinetics of receptor behavior and the mechanism of BZD-positive modulation in the presence of intact desensitization. Given that the intravenous anesthetic etomidate has been similarly shown to increase partial agonist efficacy and directly activate the channel at high concentrations (Rüsch

et al., 2004), this model may also be useful for describing the mechanism of various anesthetics. Finally, the binary elements allosteric-kinetic model representation used here provides a comprehensive approach for building and constraining nonequilibrium kinetic models incorporating multiple allosteric sites. Such models are becoming increasingly important for understanding the behavior of systems such as ion channels that are subject to modulation by numerous allosteric stimuli, including both physiological modulators and therapeutic agents.

This work was supported by the American Epilepsy Society and the Lennox Trust Fund (to M.P. Goldschen-Ohm), the Betty J. Bamforth Research Professorship, the Ralph M. Waters Distinguished Professorship (to R.A. Pearce), National Institutes of Health grant GM55719 (to R.A. Pearce), NIH grant NS046378 (to M.V. Jones), and the Department of Anesthesiology at the University of Wisconsin-Madison. A. Haroldson is presently at Dart Neuroscience LLC.

The authors declare no competing financial interests.

Author contributions: R.A. Pearce conceived the study, M.P. Goldschen-Ohm and R.A. Pearce developed the binary elements model parameterization, M.P. Goldschen-Ohm and R.A. Pearce developed the simulation software, and M.P. Goldschen-Ohm provided the graphical interfaces to the software. R.A. Pearce performed initial simulations for a precursor to scheme I, and M.P. Goldschen-Ohm performed all subsequent simulations for schemes I–VI. M.P. Goldschen-Ohm and R.A. Pearce wrote the manuscript. M.P. Goldschen-Ohm and A. Haroldson performed the experiments in the laboratory of M.V. Jones.

Kenton J. Swartz served as editor.

Submitted: 14 February 2014
Accepted: 22 May 2014

REFERENCES

Bai, D., P.S. Pennefather, J.F. MacDonald, and B.A. Orser. 1999. The general anesthetic propofol slows deactivation and desensitization of GABA(A) receptors. *J. Neurosci.* 19:10635–10646.

Benkwitz, C., M.I. Banks, and R.A. Pearce. 2004. Influence of GABAA Receptor γ2 Splice Variants on Receptor Kinetics and Isoflurane Modulation. *Anesthesiology.* 101:924–936. http://dx.doi.org/10.1097/00000542-200410000-00018

Bergmann, R., K. Kongsbak, P.L. Sørensen, T. Sander, and T. Balle. 2013. A Unified Model of the $GABA_A$ Receptor Comprising Agonist and Benzodiazepine Binding Sites. *PLoS ONE.* 8:e52323. http://dx.doi.org/10.1371/journal.pone.0052323

Boileau, A.J., and C. Czajkowski. 1999. Identification of transduction elements for benzodiazepine modulation of the GABA(A) receptor: three residues are required for allosteric coupling. *J. Neurosci.* 19:10213–10220.

Boileau, A.J., A.M. Kucken, A.R. Evers, and C. Czajkowski. 1998. Molecular dissection of benzodiazepine binding and allosteric coupling using chimeric γ-aminobutyric acidA receptor subunits. *Mol. Pharmacol.* 53:295–303.

Campo-Soria, C., Y. Chang, and D.S. Weiss. 2006. Mechanism of action of benzodiazepines on GABAA receptors. *Br. J. Pharmacol.* 148:984–990. http://dx.doi.org/10.1038/sj.bjp.0706796

Chowdhury, S., and B. Chanda. 2010. Deconstructing thermodynamic parameters of a coupled system from site-specific observables. *Proc. Natl. Acad. Sci. USA.* 107:18856–18861. http://dx.doi.org/10.1073/pnas.1003609107

Chowdhury, S., and B. Chanda. 2012. Estimating the voltage-dependent free energy change of ion channels using the median voltage for activation. *J. Gen. Physiol.* 139:3–17. http://dx.doi.org/10.1085/jgp.201110722

Chowdhury, S., and B. Chanda. 2013. Free-energy relationships in ion channels activated by voltage and ligand. *J. Gen. Physiol.* 141:11–28. http://dx.doi.org/10.1085/jgp.201210860

Colquhoun, D., and A.G. Hawkes. 1995. A Q-matrix cookbook. *In* Single-Channel Recording. B. Sakmann and E. Neher, editors. Plenum Press, New York. 589–633. http://dx.doi.org/10.1007/978-1-4419-1229-9_20

Colquhoun, D., K.A. Dowsland, M. Beato, and A.J.R. Plested. 2004. How to impose microscopic reversibility in complex reaction mechanisms. *Biophys. J.* 86:3510–3518. http://dx.doi.org/10.1529/biophysj.103.038679

Downing, S.S., Y.T. Lee, D.H. Farb, and T.T. Gibbs. 2005. Benzodiazepine modulation of partial agonist efficacy and spontaneously active GABA(A) receptors supports an allosteric model of modulation. *Br. J. Pharmacol.* 145:894–906. http://dx.doi.org/10.1038/sj.bjp.0706251

Eyring, H. 1935. The Activated Complex in Chemical Reactions. *J. Chem. Phys.* 3:107. http://dx.doi.org/10.1063/1.1749604

Franks, N.P., and W.R. Lieb. 1994. Molecular and cellular mechanisms of general anaesthesia. *Nature.* 367:607–614. http://dx.doi.org/10.1038/367607a0

Gielen, M.C., M.J. Lumb, and T.G. Smart. 2012. Benzodiazepines Modulate $GABA_A$ Receptors by Regulating the Preactivation Step after GABA Binding. *J. Neurosci.* 32:5707–5715. http://dx.doi.org/10.1523/JNEUROSCI.5663-11.2012

Goldschen-Ohm, M.P., D.A. Wagner, S. Petrou, and M.V. Jones. 2010. An Epilepsy-Related Region in the $GABA_A$ Receptor Mediates Long-Distance Effects on GABA and Benzodiazepine Binding Sites. *Mol. Pharmacol.* 77:35–45. http://dx.doi.org/10.1124/mol.109.058289

Goldschen-Ohm, M.P., D.A. Wagner, and M.V. Jones. 2011. Three Arginines in the $GABA_A$ Receptor Binding Pocket Have Distinct Roles in the Formation and Stability of Agonist- versus Antagonist-Bound Complexes. *Mol. Pharmacol.* 80:647–656. http://dx.doi.org/10.1124/mol.111.072033

Haas, K.F., and R.L. Macdonald. 1999. $GABA_A$ receptor subunit γ2 and δ subtypes confer unique kinetic properties on recombinant $GABA_A$ receptor currents in mouse fibroblasts. *J. Physiol.* 514:27–45. http://dx.doi.org/10.1111/j.1469-7793.1999.027af.x

Jackson, M.B. 1993. Activation of receptors directly coupled to ion channels. *In* Thermodynamics of Membrane Receptors and Channels. Meyer Jackson, editor. CRC Press, Boca Raton, Florida. 249–294.

Jones, M.V., and G.L. Westbrook. 1995. Desensitized states prolong GABAA channel responses to brief agonist pulses. *Neuron.* 15:181–191. http://dx.doi.org/10.1016/0896-6273(95)90075-6

Kaczorowski, G.J., O.B. McManus, B.T. Priest, and M.L. Garcia. 2008. Ion channels as drug targets: the next GPCRs. *J. Gen. Physiol.* 131:399–405. http://dx.doi.org/10.1085/jgp.200709946

Keramidas, A., and N.L. Harrison. 2008. Agonist-dependent Single Channel Current and Gating in $\alpha_4\beta_2\delta$ and $\alpha_1\beta_2\gamma_{2S}$ $GABA_A$ receptors. *J. Gen. Physiol.* 131:163–181. http://dx.doi.org/10.1085/jgp.200709871

Keramidas, A., and N.L. Harrison. 2010. The activation mechanism of $\alpha_1\beta_2\gamma_{2S}$ and $\alpha_3\beta_3\gamma_{2S}$ $GABA_A$ receptors. *J. Gen. Physiol.* 135:59–75. http://dx.doi.org/10.1085/jgp.200910317

Kloda, J.H., and C. Czajkowski. 2007. Agonist-, Antagonist-, and Benzodiazepine-Induced Structural Changes in the α_1 Met^{113}-Leu^{132} region of the $GABA_A$ receptor. *Mol. Pharmacol.* 71:483–493. http://dx.doi.org/10.1124/mol.106.028662

Koshland, D.E. Jr., G. Némethy, and D. Filmer. 1966. Comparison of experimental binding data and theoretical models in proteins

containing subunits. *Biochemistry.* 5:365–385. http://dx.doi.org/10.1021/bi00865a047

Lavoie, A.M., and R.E. Twyman. 1996. Direct evidence for diazepam modulation of GABAA receptor microscopic affinity. *Neuropharmacology.* 35:1383–1392.

Li, P., M.M. Eaton, J.H. Steinbach, and G. Akk. 2013. The benzodiazepine diazepam potentiates responses of α1β2γ2L γ-aminobutyric acid type A receptors activated by either γ-aminobutyric acid or allosteric agonists. *Anesthesiology.* 118:1417–1425. http://dx.doi.org/10.1097/ALN.0b013e318289bcd3

Li, X., and R.A. Pearce. 2000. Effects of Halothane on $GABA_A$ Receptor Kinetics: Evidence for Slowed Agonist Unbinding. *J. Neurosci.* 20:899–907.

Macdonald, R.L., and R.W. Olsen. 1994. $GABA_A$ Receptor Channels. *Annu. Rev. Neurosci.* 17:569–602. http://dx.doi.org/10.1146/annurev.ne.17.030194.003033

Maksay, G. 1994. Thermodynamics of γ-Aminobutyric Acid Type A Receptor Binding Differentiate Agonists from Antagonists. *Mol. Pharmacol.* 46:386–390.

Mellor, J.R., and A.D. Randall. 1997. Frequency-Dependent Actions of Benzodiazepines on $GABA_A$ Receptors in Cultured Murine Cerebellar Granule Cells. *J. Physiol.* 503:353–369. http://dx.doi.org/10.1111/j.1469-7793.1997.353bh.x

Monod, J., J. Wyman, and J.P. Changeux. 1965. On the nature of allosteric transitions: a plausible model. *J. Mol. Biol.* 12:88–118. http://dx.doi.org/10.1016/S0022-2836(65)80285-6

Mozrzymas, J.W., A. Barberis, K. Mercik, and E.D. Zarnowska. 2003. Binding sites, singly bound states, and conformation coupling shape GABA-evoked currents. *J. Neurophysiol.* 89:871–883. http://dx.doi.org/10.1152/jn.00951.2002

O'Shea, S.M., L.C. Wong, and N.L. Harrison. 2000. Propofol increases agonist efficacy at the GABA(A) receptor. *Brain Res.* 852:344–348.http://dx.doi.org/10.1016/S0006-8993(99)02151-4

Perrais, D., and N. Ropert. 1999. Effect of zolpidem on miniature IPSCs and occupancy of postsynaptic GABAA receptors in central synapses. *J. Neurosci.* 19:578–588.

Press, W.H., S.A. Teukolsky, W.T. Vetterling, and B.P. Flannery. 2007. Integration of ordinary differential equations. *In* Numerical Recipes 3rd Edition: The Art of Scientific Computing. Cambridge University Press, Cambridge. 1235.

Pritchett, D.B., H. Sontheimer, B.D. Shivers, S. Ymer, H. Kettenmann, P.R. Schofield, and P.H. Seeburg. 1989. Importance of a novel $GABA_A$ receptor subunit for benzodiazepine pharmacology. *Nature.* 338:582–585. http://dx.doi.org/10.1038/338582a0

Rogers, C.J., R.E. Twyman, and R.L. Macdonald. 1994. Benzodiazepine and β-carboline regulation of single $GABA_A$ receptor channels of mouse spinal neurones in culture. *J. Physiol.* 475:69–82.

Rudolph, U., and F. Knoflach. 2011. Beyond classical benzodiazepines: novel therapeutic potential of $GABA_A$ receptor subtypes. *Nat. Rev. Drug Discov.* 10:685–697. http://dx.doi.org/10.1038/nrd3502

Rüsch, D., and S.A. Forman. 2005. Classic Benzodiazepines Modulate the Open-Close Equilibrium in α1β2γ2L γ-Aminobutyric Acid Type A Receptors. *Anesthesiology.* 102:783–792. http://dx.doi.org/10.1097/00000542-200504000-00014

Rüsch, D., H. Zhong, and S.A. Forman. 2004. Gating Allosterism at a Single Class of Etomidate Sites on $\alpha_1\beta_2\gamma_{2L}$ $GABA_A$ Receptors Accounts for Both Direct Activation and Agonist Modulation. *J. Biol. Chem.* 279:20982–20992. http://dx.doi.org/10.1074/jbc.M400472200

Sharkey, L.M., and C. Czajkowski. 2008. Individually monitoring ligand-induced changes in the structure of the GABAA receptor at benzodiazepine binding site and non-binding-site interfaces. *Mol. Pharmacol.* 74:203–212. http://dx.doi.org/10.1124/mol.108.044891

Sieghart, W. 1995. Structure and Pharmacology of γ-Aminobutyric $Acid_A$ Receptor Subtypes. *Pharmacol. Rev.* 47:181–234.

Sigg, D. 2013. A linkage analysis toolkit for studying allosteric networks in ion channels. *J. Gen. Physiol.* 141:29–60. http://dx.doi.org/10.1085/jgp.201210859

Topf, N., A. Jenkins, N. Baron, and N.L. Harrison. 2003. Effects of Isoflurane on γ-Aminobutyric Acid Type A Receptors Activated by Full and Partial Agonists. *Anesthesiology.* 98:306–311. http://dx.doi.org/10.1097/00000542-200302000-00007

Twyman, R.E., C.J. Rogers, and R.L. Macdonald. 1989. Differential regulation of γ-aminobutyric acid receptor channels by diazepam and phenobarbital. *Ann. Neurol.* 25:213–220. http://dx.doi.org/10.1002/ana.410250302

Vicini, S., J.M. Mienville, and E. Costa. 1987. Actions of Benzodiazepine and β-Carboline Derivatives on γ-Aminobutyric Acid-Activated Cl^- Channels Recorded from Membrane Patches of Neonatal Rat Cortical Neurons in Culture. *J. Pharmacol. Exp. Ther.* 243:1195–1201.

Wagner, D.A., C. Czajkowski, and M.V. Jones. 2004. An Arginine Involved in GABA Binding and Unbinding But Not Gating of the $GABA_A$ Receptor. *J. Neurosci.* 24:2733–2741. http://dx.doi.org/10.1523/JNEUROSCI.4316-03.2004

Wieland, H.A., H. Lüddens, and P.H. Seeburg. 1992. A single histidine in GABAA receptors is essential for benzodiazepine agonist binding. *J. Biol. Chem.* 267:1426–1429.